Exploiting Dispersion Effect of Signals for Accurate Indoor WiFi Localization

YIMIAO SUN, School of Software and BNRist, Tsinghua University, Beijing, China
YUAN HE*, School of Software and BNRist, Tsinghua University, Beijing, China
JIACHENG ZHANG, School of Software and BNRist, Tsinghua University, Beijing, China
XIN NA, School of Software and BNRist, Tsinghua University, Beijing, China
YANDE CHEN, School of Software and BNRist, Tsinghua University, Beijing, China
WEIGUO WANG, School of Software and BNRist, Tsinghua University, Beijing, China
XIUZHEN GUO, College of Control Science and Engineering, Zhejiang University, Hangzhou, China

WiFi-based device localization is a key technology for smart applications, while most of which rely on LoS signals to work. However, in real-world indoor environments, very few LoS signals are usable for accurate localization. This paper presents Bifrost, a novel hardware-software co-design to cope with this practical problem. The core idea of Bifrost is to reinvent WiFi signals to provide sufficient LoS signals. Specifically, we present a low-cost plug-in design of leaky wave antenna (LWA) that can generate orthogonal polarized signals: On one hand, LWA disperses signals of different frequencies to different angles, thus providing AoA information for the localized target. On the other hand, the target further leverages the antenna polarization mismatch to distinguish AoAs from different LWAs. Besides, fine-grained information in CSI is exploited to mitigate multipath and noise. Besides, a dedicated Kalman filter is proposed to facilitate the cooperation of Bifrost and SpotFi, a state-of-the-art approach, to enhance the availability and accuracy of SpotFi. The evaluation results show that the median localization error of Bifrost is 0.81m, 52.35% less than that of SpotFi. When combined with Bifrost to work in realistic settings, SpotFi can reduce the localization error by 33.54%.

CCS Concepts: • **Information systems** → **Location based services**; • **Networks** → **Location based services**; • **Computer systems organization** → *Embedded systems.*

Additional Key Words and Phrases: WiFi Localization, Indoor Localization, Leaky Wave Antenna, Dispersion Effect, RF Computing

1 Introduction

Location information is crucial for the function of IoT devices [17, 31, 40, 44], especially for smart indoor applications, such as smart home [28, 36], indoor navigation [11, 32, 38] and so on. Due to the ubiquitous deployment of WiFi access points (APs) and wide availability of WiFi modules on the devices, WiFi-based

*Corresponding author.

Authors' Contact Information: Yimiao Sun, School of Software and BNRist, Tsinghua University, Beijing, Beijing, China; e-mail: sym21@mails.tsinghua.edu.cn; Yuan He, School of Software and BNRist, Tsinghua University, Beijing, Beijing, China; e-mail: heyuan@tsinghua.edu.cn; Jiacheng Zhang, School of Software and BNRist, Tsinghua University, Beijing, Beijing, China; e-mail: zhangjc21@mails.tsinghua.edu.cn; Xin Na, School of Software and BNRist, Tsinghua University, Beijing, Beijing, China; e-mail: nx20@mails.tsinghua.edu.cn; Yande Chen, School of Software and BNRist, Tsinghua University, Beijing, Beijing, China; e-mail: cyd22@mails.tsinghua.edu.cn; Weiguo Wang, School of Software and BNRist, Tsinghua University, Beijing, Beijing, China; e-mail: wwg18@mails.tsinghua.edu.cn; Xiuzhen Guo, College of Control Science and Engineering, Zhejiang University, Hangzhou, Zhejiang, China; e-mail: guoxiuzhen94@gmail.com.

ACM 1550-4867/2025/3-ART
https://doi.org/10.1145/3725850

(a) (b)

Fig. 1. A model-driven method works well when (a) sufficient LoS signals are available but becomes inaccurate when (b) NLoS signals have to be used.

localization [15, 30, 42, 45] appears to be promising for indoor localization. Existing works of WiFi-based indoor localization can be broadly grouped into two categories, data-driven methods and model-driven methods.

Data-driven methods are typically represented by fingerprint [6, 23, 35]. These methods need to collect Received Signal Strength (RSS) or CSI at different places to construct a database mapping RSS (or CSI) with locations, which is a labor-intensive process. Also, their performance may be vulnerable to dynamic environments.

Model-driven methods induce less labor cost and attract more research studies. Generally, a model-driven method calculates the location by estimating signals' Angle-of-Arrival (AoA) [8, 14, 39], Time-of-Flight (ToF) [40, 44] or both [9, 22]. Most of the existing approaches rely on Line-of-Sight (LoS) signals to work, as Fig. 1(a) illustrates, while a critical problem is often neglected: In the real-world indoor environments, WiFi signals are everywhere, but very few of them are usable for accurate localization. As an example to validate this finding, Fig. 2 plots the statistics of the real deployment of WiFi APs in a library (48 rooms) and an office building (54 rooms). The data shows that in nearly half of all the rooms, there is not even one LoS AP available. The rooms with sufficient LoS signals account for less than 5% of all the rooms. In other words, the chance for a WiFi device to receive sufficient LoS WiFi AP signals, namely the case for it to be accurately localized by using an existing approach, is less than 5%. That well explains why the practical performance of using the existing localization approaches is far from being satisfactory.

A straightforward idea to address the above problem is to increase the number of deployed WiFi APs, until everywhere is covered by at least 3 LoS APs. It isn't practical, however. Taking the library and office building investigated in Fig. 2 as an example, typically there are 50 rooms in a building. Covering every room with 3 APs requires 150 APs to be deployed, which means multiple drawbacks, such as substantial deployment cost of cables (connecting the APs), overly crowded wireless spectrum, and frequent interference and collisions in the wireless communication.

This paper presents a novel approach called Bifrost[1], a plug-and-play and cost-effective scheme to significantly enhance the availability of LoS WiFi signals and in turn the localization accuracy. In light of the research progress on leaky wave antenna (LWA) in recent years [12, 13, 21], Bifrost exploits dispersion effect of wireless signals [19]. Deployed in the space covered by WiFi signals, a LWA can receive those signals and then radiate them at different frequencies towards different directions, exhibiting frequency and spatial division multiplexing (FSDM) features, as is reinventing WiFi signals.

Fig. 3 illustrates the high-level principle of Bifrost. To localize a target device, Bifrost uses two LWAs to transform WiFi signals into FSDM signals, so the target device will receive two LoS FSDM signals with a unique pair of frequencies. Since the frequency and the propagation direction of FSDM signals are coupled, the target device can estimate its AoAs to both LWAs by analyzing the received spectrum and then calculate its location.

Compared with using WiFi APs, using LWA to assist localization offers the following two distinct advantages:

[1]In Norse mythology, Bifrost is a rainbow bridge that reaches between Midgard (Earth) and Asgard (the realm of gods).

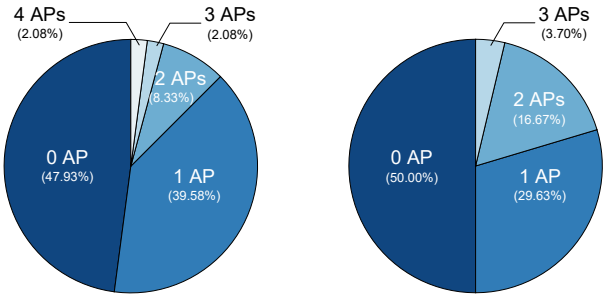

(a) Library (48 rooms) (b) Office (54 rooms)

Fig. 2. The number of LoS APs in each room in a library and an office building.

1) **Cost-effective.** The cost of a LWA in Bifrost is 7.41 USD (4.36 USD for the material and 3.05 USD for the control module), which is significantly lower than that of a WiFi AP (typically 30 ~ 100 USD [1, 2]).
2) **Easy to use.** Deploying a LWA is very convenient. It can operate in a plug-and-play manner without the need to connect power cables.

Leveraging these two advantages, Bifrost can be easily implemented in any environment with WiFi coverage, no matter whether the WiFi signals are LoS or not. Bifrost can either work independently, or cooperatively with other conventional WiFi-based localization methods.

The design of Bifrost tackles several critical challenges, which are summarized as follows:

Ambiguity between different LWAs. As Fig. 3 shows, a target device may receive signals from two LWAs, which are reinvented from the same WiFi signal source. Without a special design, it is almost impossible for the target to distinguish one LWA from the other. To overcome this problem, the LWAs in Bifrost are designed to generate orthogonal circular polarized (CP) signals, so that they won't mix up with each other (§3.1). Polarization of LWA signals can be conveniently switched by altering the input port of WiFi signals, without the need for reconstruction or modifications to the LWA's structure.

Signal Extraction from the interfered frequency band. Since FSDM signals radiated by LWAs are transformed from existing WiFi signals, the two types of signals operate within the same frequency band and can be simultaneously received by a target device. Directly using such signals leads to erroneous AoA estimation. To deal with such interference, LWAs in Bifrost work in a duty-cycled manner. The target device is able to detect distinctive variation of the signal amplitude at the frequencies of FSDM signals (§3.3). By analyzing WiFi CSI, the target device can effectively extract the desired FSDM signals from interfered frequency band.

Indoor multipath effect. The multipath effect in the indoor environment may seriously affect the quality of the received FSDM signals and further affect the localization accuracy. In order to identify FSDM signals propagating along the LoS path, Bifrost operates in two steps. First, we map frequencies of FSDM signals with subcarriers in CSI and cluster adjacent subcarriers to only retain the cluster with the highest energy (§3.4). Second, we take the intersection of two clusters (corresponding to the two orthogonal CP signals), and determine the final frequency by weighting the center frequency of the clustered subcarriers (§3.5).

The idea of Bifrost has been preliminary explored in our previous work [34], and we have carried out further extensions and explorations in this version. Compared with the published SenSys version, we first design an algorithm to combine Bifrost and SpotFi to work cooperatively to increase the localization accuracy and the availability of the indoor WiFi localization system (§4). Then we elaborate on a series of practical issues concerning the applicability of Bifrost, including reciprocity of LWAs, polarization alteration, *etc* (§5). Finally, we conduct a series of experiments to study the performance enhancement when Bifrost works cooperatively with SpotFi, and the impact of human activity on the performance of Bifrost (§6.2).

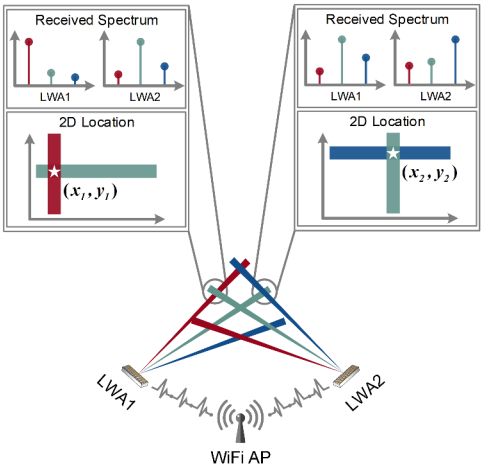

Fig. 3. The high-level principle of Bifrost.

Our contributions can be summarized as follows:

1) We tackle a significant problem, namely the limited availability of LoS signals, which is overlooked by the existing works on WiFi-based indoor localization. We reinvent WiFi signals by exploiting the dispersion effect, which represents a new direction of utilizing LWAs.
2) We address a series of non-trivial challenges, such as signal ambiguity, interference, and multipath effect, *etc.* The design of Bifrost effectively ensures the quality of signals used for localization.
3) We propose an algorithm to facilitate the cooperation of Bifrost and SpotFi, a state-of-the-art approach, to reduce the error and enhance the availability of indoor WiFi localization.
4) We implement Bifrost and evaluate its performance under various settings. The results show that the median localization error of Bifrost is 0.81m, which is 52.35% less than that of SpotFi, a state-of-the-art approach. SpotFi, when combined with Bifrost to work in realistic settings, can reduce the localization error by 33.54%.

This paper proceeds as follows: §2 introduces background knowledge on the signal polarization and the LWA. Then §3 unfolds the design of Bifrost in both hardware and software. §4 elaborates on how to facilitate the cooperation of Bifrost and SpotFi. Some practical issues are discussed in §5. The implementation and evaluation results are presented in §6. We discuss practical issues in §7 and summarize related works in §8. This work is concluded in §9.

2 Primer

This section introduces preliminary knowledge of our work: polarization of wireless signals and leaky wave antenna.

2.1 Signal Polarization

Polarization is a fundamental property of wireless signals, including FSDM and WiFi signals investigated inf this work. As Fig. 4 shows, there are three kinds of different polarization, *i.e.*, linear polarization (LP), circular polarization (CP) and elliptical polarization (EP). CP signal can be further divided into left-hand circular polarization (LHCP) and right-hand circular polarization (RHCP), which are orthogonal and won't interfere with each other.

The polarization of a signal is accorded with that of its transmitting antenna but may change during propagation. To ensure effective reception, it should match the polarization of the receiving antenna, partially at least. The CP signal can be decomposed into two orthogonal LP signals. Thus, the LP antenna can only receive the component

(a) (b) (c)

Fig. 4. The properties of polarized electromagnetic waves: (a) Linear polarization (LP); (b) Circular polarization (CP); (c) Elliptical polarization (EP).

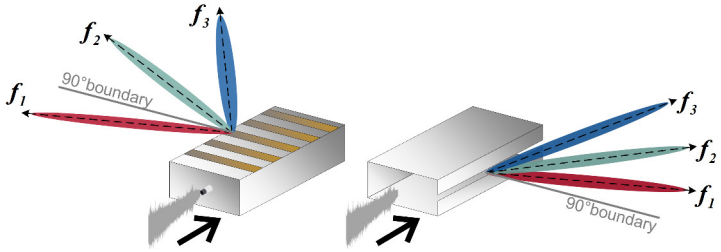

(a) Periodic structure. (b) Uniform structure.

Fig. 5. Typical structures of leaky wave antenna[2].

whose polarization direction is parallel to itself but loses half of the signal energy. Similarly, the CP antenna can only receive half of the LP signal's energy. However, when LHCP antenna is used to receive RHCP signals or vice versa, RSS is theoretically zero because these two polarizations are orthogonal. That is the reason why Bifrost can eliminate the ambiguity of two FSDM signals radiated from different LWAs.

2.2 Leaky Wave Antenna

LWA belongs to the class of traveling-wave antennas, where the propagating wave inside the antenna structure can "leak" (*i.e.,* radiate) from the waveguide to the free space [27]. It can couple the leaky wave's frequency and radiation direction to produce a frequency and spatial division multiplexing (FSDM) signal, as shown in Fig. 5. Specifically, direction of the signal $\overrightarrow{E_f}$ with frequency f can be determined by [41]:

$$\theta(f) = \arccos\left[\frac{\beta(f)}{k_0(f)}\right], \tag{1}$$

where $\beta(f)$ and $k_0(f)$ are the phase constant along the LWA and the propagation constant in the free space *w.r.t* $\overrightarrow{E_f}$ [27].

Currently, two main types of LWAs have been extensively studied. 1) *The uniform LWA*, which employs a metallic waveguide with a slit cut along its length [12, 21], as depicted in Fig. 5(b). The FSDM signal leaked from a uniform LWA can only propagate towards the forward region (*i.e.,* $[0°, 90°]$). 2) *The periodic LWA*, which is typically designed using a dielectric substrate with a periodic array of metal strips (*i.e.,* slots) [4, 5] and similar to an antenna array, as shown in Fig. 5(a). The FSDM signal of this type of LWA can propagate towards both forward and backward regions (*i.e.,* $[0°, 180°]$) [19].

[2]It's worth noting that the 2D radiation pattern is used here for illustration purposes. In reality, the radiation pattern of the leaky wave with a specific frequency is more like a cone, with a generatrix along the propagation direction of the traveling wave.

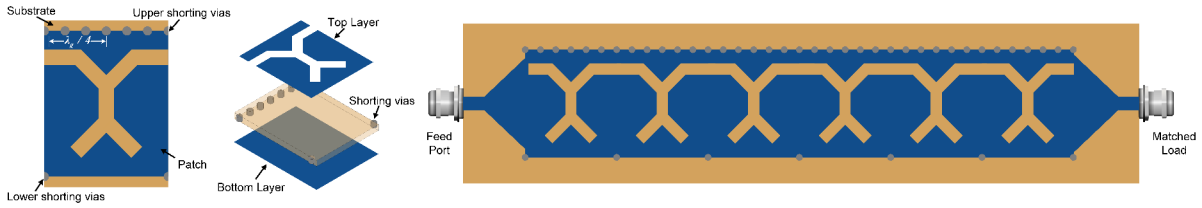

(a) Unit. (b) Layered structure. (c) Complete design.

Fig. 6. General view of CPLWA used in Bifrost.

Periodic LWA has been widely studied in recent research due to its versatile slot design and low-cost fabrication using the printed circuit board (PCB) process. These attributes have made it a popular choice in various applications. Bifrost also employs the periodic structure to produce circular polarized signals.

3 Bifrost

In this section, we first articulate how to design the circular polarized LWA (*i.e.,* CPLWA) to transform the input LP signal into the CP signal with the FSDM feature. Then, we present the details of our approach of localization with the CPLWA.

3.1 CPLWA Design

Unlike many traditional LWAs [3, 5], Bifrost utilizes CP[3] (*i.e.,* RHCP and LHCP) to distinguish different LWAs and corresponding FSDM signals. We specially design a CPLWA that can generate both LHCP and RHCP signals. As shown in Fig. 6(a), our CPLWA has both vertical and horizontal slots to generate orthogonal LP signals, and further to form the CP signal (the bifurcation is designed for performance optimization). Denoting the guided wavelength at 5.25GHz of the substrate material is λ_g, the distance between the center of horizontal and vertical slots is $\frac{\lambda_g}{4}$.

In the fabrication process of CPLWA, we adopt a two-layer copper-clad substrate structure, as shown in Fig. 6(b). The substrate material is F4BM-2, whose permittivity $\epsilon = 3.02$. The top and bottom layers of the substrate consist of copper and have undergone tin immersion plating to prevent oxidation. The bottom layer of copper functions as the ground, and the shorting vias are incorporated to penetrate the substrate, connecting the top and bottom layers in order to ground the top layer.

The final structure of our proposed CPLWA is depicted in Fig. 6(c), where multiple units are linearly arranged together to enhance the directivity of the FSDM signal, which is similar to the antenna array. Note that a CPLWA is composed of 6 units as an illustration, but 11 units are arranged in practice. This CPLWA features two ports on both ends: one is the feed port that connects to an LP antenna for absorbing the WiFi signal, and the other should connect to a matched 50Ω load. By changing the signal feed port, polarization of the FSDM signal can switch between LHCP and RHCP. If the input signal has gone through all slots and reached the other end, yet still has energy remaining, the matched load will absorb the excess signal.

The CPLWA used in Bifrost is specially designed at 5.17GHz-5.33GHz WiFi band, while this structure and design methodology are universally applicable for other frequencies and bandwidths.

Now we conduct a quick validation to show the key performance of the proposed CPLWA using ANSYS HFSS. Firstly, the direction of the FSDM signal *w.r.t* different frequencies is depicted in Fig. 7(a). There is a total 22° field of view (FoV) across the operating frequency band (5.17GHz-5.33GHz). Note that when the LP signal is fed into

[3]Unless otherwise specified, CP signals stand for both RHCP and LHCP signals.

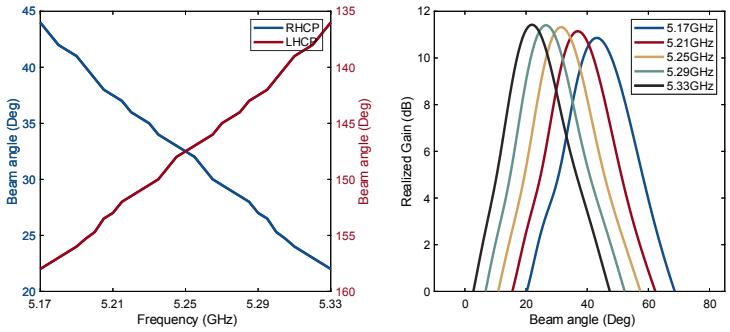

(a) Main beam direction. (b) Realized gain.

Fig. 7. Key results of the CPLWA.

the right port or left port, the RHCP or LHCP signal will be radiated from 22° to 44° or 136° to 158°, respectively. Fig. 7(b) shows the energy distribution of signals at five different frequencies. It is evident that the energy of the leaky signal concentrates on the correct direction, and their realized gains are all above 11.5dB. Therefore, the direction can be easily identified by examining the signal energy.

3.2 Basic Localization Model

Let S_l and S_r respectively denote LHCP and RHCP signals that propagate from corresponding LWAs to the target via the LoS paths. The frequencies of these two signals, f_l and f_r, are what we desire for calculating the location. Recall that S_l and S_r are featured in frequency and space division multiplexing (FSDM) and orthogonal CP[4], so these two signals won't interfere with each other. As a result, the target can estimate its relative direction to both LWAs based on the received spectrum and the radiation pattern of the two LWAs. Further, given locations of two LWAs, $L_r\ (x_r, y_r, z_r)$ of the RHCP LWA and $L_l\ (x_l, y_l, z_l)$ of the LHCP LWA, the target can output its absolute location. In detail, as we mentioned in §2, the radiation pattern of the LWA is a conical surface at a specific frequency. Therefore, the location $L_t\ (x_t, y_t)$ of the target device is the intersection point of the two conical surfaces and the horizontal plane of its height. By combining these conditions, L_t can be estimated by solving the following equation set:

$$L_t = (x_t, y_t) = \begin{cases} F(L_r, f_r)\,, \\ F(L_l, f_l)\,, \\ z = z_t \end{cases} \tag{2}$$

where z_t is the target's height; functions $F(L_r, f_r)$ and $F(L_l, f_l)$ are mathematical equations of conical surfaces with the location of LWAs as the vertex. These two equations indicate the propagation directions of RHCP and LHCP signals at frequencies f_r and f_l, respectively. Taking the RHCP signal as an example, $F = F(L_r, f_r)$ can be formulated as

$$F = (x - x_r)^2 - \frac{(y - y_r)^2}{a^2} - \frac{(z - z_r)^2}{a^2}\,, \tag{3}$$

where $a = \cot\left[\theta(f_r)\right]$.

However, there are two other types of signals impacting the localization accuracy when Bifrost functions: 1) *LP WiFi signal* that is emitted by the WiFi AP, and then received by the target. This signal establishes data communication between the target and the AP and propagates in both the LoS path and multipath. It is also the

[4]Unless stated otherwise, CP signals have the property of FSDM.

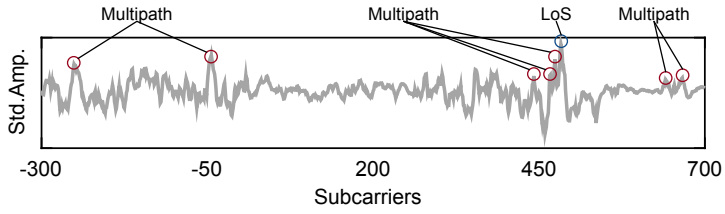

(a) Normalized amplitude variation.

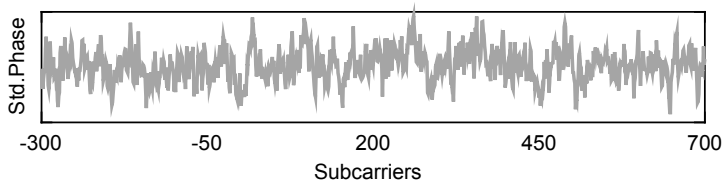

(b) Normalized phase variation.

Fig. 8. Standardized CSI variation.

input signal of LWAs, which will be transformed into FSDM signals. 2) *CP multipath signal* that propagates from LWAs to the target after reflection, resulting in noisy signals at the target.

Thus, we should first identify the frequency of the FSDM signal from the *LP WiFi signal* (discussed in §3.3) and then filter out the *CP multipath signal* as much as possible (discussed in §3.4 and §3.5), to accurately estimate frequencies, f_l and f_r, and the target's location.

3.3 Identifying Frequencies of CP signals

When Bifrost functions, LWAs need the LP WiFi signal as input, and the target device may also need it for data communication with the WiFi AP. Nevertheless, the LP signal may interfere with the reception of the CP signal, because CP antennas at the target device can receive the LP signal (as already explained in §2). To cancel this interference, we control LWAs to be periodically turned on and off, working in a duty-cycled manner. This design allows the target to identify frequencies that correspond to the CP signal by analyzing the variation in its received spectrum, and at the same time, saves energy of LWAs. Specifically, we exploit WiFi CSI to explore fine-grained information on the amplitude and phase of the subcarriers. Fig. 8 illustrates the result of a proof-of-concept experiment, where subcarriers correspond to LoS and multipath signals are distinguishable in the normalized amplitude of CSI. However, the variation in phase is not obvious, making it challenging to discern useful subcarriers because they are often obscured by random errors and noise. Thus, we can only extract frequencies of the CP signal based on the amplitude variation in CSI.

As a LWA turns on or off, we denote the corresponding CSI as $H_{on}(f_k)$ and $H_{off}(f_k)$ for the k-th subcarrier with center frequency f_k, respectively. The former is jointly influenced by CP and LP signals, while the latter is determined by the LP signal only, leading to the following relationship:

$$\begin{aligned} \|H_{on}(f_k)\| &= \|H^{CP}(f_k) + H^{LP}(f_k)\|, \\ \|H_{off}(f_k)\| &= \|H^{LP}(f_k)\|, \end{aligned} \tag{4}$$

where $\|H^{CP}(f_k)\|$ is the amplitude of subcarriers corresponding to the CP signal, and $\|H^{LP}(f_k)\|$ is that of the LP signal. Based on these two values, we can quantify the variation of CSI caused by the CP signal:

$$\|\Delta H(f_k)\| = \|H_{on}(f_k)\| - \|H_{off}(f_k)\| \tag{5}$$

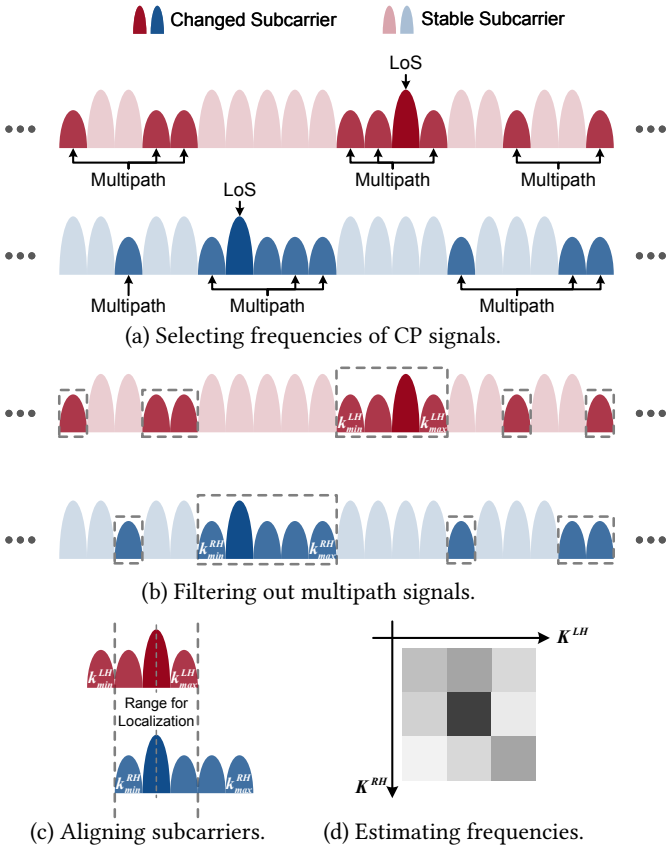

(a) Selecting frequencies of CP signals.

(b) Filtering out multipath signals.

(c) Aligning subcarriers.

(d) Estimating frequencies.

Fig. 9. Workflow of selecting correct frequencies (LHCP and RHCP are distinguished by red and blue colors).

In order to accurately analyze this variation and mitigate the effect of occasional outliers and noise, a Z-Score normalization procedure is performed on $\|\Delta H(f_k)\|$. We execute a preliminary screening to quickly filter out the subcarriers that are less likely corresponding to the frequencies of the CP signals. A percentage threshold $\varepsilon \in [0, 1]$ is set to select subcarriers with a larger value of $\|\Delta H(f_k)\|$, indicating that these subcarriers undergo significant changes and are more likely to be affected by the CP signal. The value of ε is chosen empirically based on the degree of multipath. Fig. 9(a) shows a high-level overview of the selected subcarriers, where LHCP and RHCP signals are highlighted in red and blue, respectively. In subsequent stages, we exclusively focus on these selected subcarriers.

3.4 Filtering out the Multipath Signal

As shown in Fig. 8(a), even though we have identified the frequencies of the CP signal from the WiFi signal, there still exists the multipath signal, resulting in undesired variation in $\|\Delta H(f_k)\|$. Note that the multipath signal is mainly introduced by reflection of the CP FSDM signal. We find that subcarriers corresponding to the multipath signal can be divided into two categories: 1) Sparsely clustered subcarriers C_s: FSDM signal with different frequencies and propagation directions may go through reflection at many places, but only a few of those signals reach the target with inconsecutive frequencies, resulting in many sparse clusters of subcarriers.

2) Compactly clustered subcarriers C_c: There are some FSDM signals with frequencies close to that of the LoS signal. Those FSDM signals reflect just right near the target device, which results in a compact and wide cluster of subcarriers influenced by multipath and LoS signals.

Here we first try to filter out C_s. To do so, all the varied subcarriers are clustered, respectively, as Fig. 9(b) illustrates. Then, the following integral function will be calculated for every cluster to find the one most likely to be corresponding to the LoS signal,

$$C^i = \int_{f^i_{k_{\min}}}^{f^i_{k_{\max}}} \|\Delta H(f^i_k)\| \, df^i_k \tag{6}$$

where $f^i_{k_{\min}}$ and $f^i_{k_{\max}}$ are the minimum and maximum frequencies of the $i-$th cluster, respectively. The value of C^i can be regarded as the area formed by the curve of $\|\Delta H(f^i_k)\|$ and the two frequencies $f^i_{k\min}$, $f^i_{k\max}$. The wider the bandwidth and higher the amplitude of a cluster are, the greater the value of its C^i is.

After that, we only retain the cluster that bears the highest C^i, which is most likely to be C_c and contains subcarriers corresponding to the LoS signal. However, as we mentioned before, some subcarriers in C_c are also corresponding to the undesired multipath signal. Next, we are going to purify C_c by narrowing down its frequency range as much as possible.

3.5 Purifying the LoS Signal for Localization

Denote the frequency range of C_c as $\left[k^r_{\min}, k^r_{\max}\right]$ for RHCP signals and $\left[k^l_{\min}, k^l_{\max}\right]$ for LHCP signals. In both of the two ranges, we are going to find the subcarrier with the largest $\|\Delta H(f_k)\|$ as Fig. 9(c) illustrates. After obtaining them, we denote the index of selected subcarriers as K^r and K^l. Next, as Fig. 9(c) depicts, we align K^r and K^l, then trim the head and tail to retain the intersection of two clusters, $\|\Delta H^r(f_k)\|$ and $\|\Delta H^l(f_k)\|$. Finally, we multiply $\|\Delta H^r(f_k)\|$ and $\|\Delta H^l(f_k)\|$ to form a weight matrix G, which is illustrated in Fig. 9(d).

$$G = \begin{bmatrix} \|\Delta H^r(f_{K^r-\delta})\| \\ \\ \dots \\ \\ \|\Delta H^r(f_{K^r+\delta})\| \end{bmatrix} \times \left[\|\Delta H^l(f_{K^l-\delta})\| \dots \|\Delta H^l(f_{K^l+\delta})\|\right] \tag{7}$$

where δ is half the length of $\|\Delta H^r(f_k)\|$ and $\|\Delta H^l(f_k)\|$.

Then, we estimate f_r and f_l by computing the weighted average of values in $[f_{K^r-\delta}, f_{K^r+\delta}]$ and $\left[f_{K^l-\delta}, f_{K^l+\delta}\right]$, which are weighted by the corresponding values in the matrix G. The purpose of this step is still to mitigate the interference of the multipath signal. After that, the estimated values of the two frequencies will be fed into Eq. (3) to output an estimation of the target's location.

4 Enhancing The Availability of Indoor WiFi Localization with Bifrost

In this section, we elaborate on how to extend Bifrost's ability to enhance the availability of other indoor WiFi localization methods, for example, SpotFi, a state-of-the-art approach. We first demonstrate the disability of SpotFi in the indoor environment when there is lack of LoS APs. Then we propose an algorithm to facilitate the cooperation of Bifrost and SpotFi to improve the localization accuracy when a target device is moving indoors.

Indoor scenarios likely include objects that create NLoS settings, for example, walls in rooms. Therefore, it's less likely for a device to establish LoS paths with indoor WiFi APs, according to our investigation in Fig. 2. In that case, the AoA information captured by the target device may be deviated. We conduct two groups of proof-of-concept experiment to illustrate this situation. We separate the target device and a WiFi AP with a wall, and then record the AoA estimation when the target device is moving or not. Then we set the target device and the WiFi AP in the same room to maintain LoS connection. As Fig. 10 shows, although SpotFi achieves great AoA

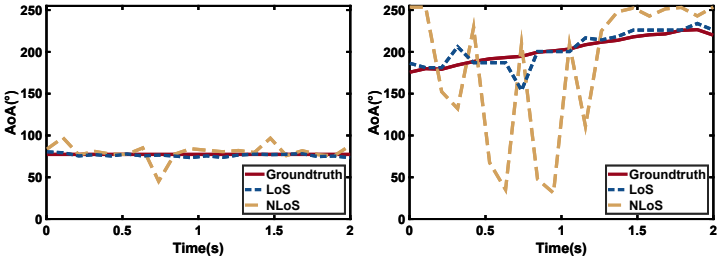

(a) Stable. (b) Mobile.

Fig. 10. AoA estimation of SpotFi when the device is stable and mobile.

estimation performance with the LoS AP, severe deviation occurs in NLoS no matter whether the target device moves. In the latter case, traditional localization with distributed WiFi APs can't work.

In order to enhance the accuracy as well as the availability of indoor WiFi localization, we propose to combine Bifrost and SpotFi to work cooperatively. Specifically, when the target device is moving indoors (*e.g.,* carried on the moving person), it can use SpotFi to calculate its location when there are at least 3 LoS APs in LoS (*i.e.,* with three stable AoA estimation), while otherwise switching to Bifrost by deploying two LWAs. To detect whether the AP is in LoS, we set a threshold to evaluate the variance of the estimated AoA in a time window. If the variance is beyond the threshold, we consider the AP in NLoS (*e.g.,* blocked by the wall). The reason is that, in the LoS scenarios, the energy of the LoS signal is much higher than that of the noise, so the variation in the noise signal doesn't affect the identification of the LoS signal. As such, the AoA estimation in LoS scenarios is relatively stable and shows a lower variance. Conversely, in the NLoS scenarios, the NLoS signal undergoes significant attenuation due to the reflection and diffraction, so its energy is comparable to that of the noise signal. As a result, the direction of the signal with the highest energy may fluctuate drastically. In that case, the AOA estimation will jitter heavily, leading to a high variance. This combination can not only increase the localization accuracy and the availability of the indoor WiFi localization system but also prevent the deployment of substantial WiFi APs.

However, when the target device moves indoors, the measured locations may experience jitter due to variations in the channel and the multipath effect, even when the device is within LoS scenarios. For instance, as shown in Fig. 10(b), despite the target device maintaining a LoS path with the WiFi AP, the measured AoA exhibits obvious jitters, which will in turn lead to errors in the estimated location. To mitigate these errors, we employ a dedicated Kalman filter, as detailed in Algorithm 1. The Kalman filter is a widely adopted method for addressing noise and jitter in measured data [29, 33]. By continuously performing cycles of prediction and update, it can provide more accurate estimates of the results.

We denote the 2D location of the target device at time t as $A_t = [x_t,\ y_t]^T$, with $A_0 = [x_0,\ y_0]^T$ being initialized with the first few points at the beginning of the movement. The predicted subsequent state vector $\hat{A}_t^{\ -}$ (*i.e.,* the a priori state estimate) can be calculated as

$$\hat{A}_t^{\ -} = F \cdot A_{t-1} \tag{8}$$

where F is the state transition matrix, and A_{t-1} is the state vector of the previous state.

Then, the target device obtains the AoA estimation sequence $S_i = [AoA_1^i\ AoA_2^i\ ...\ AoA_n^i]$ of the i-th WiFi AP in the nearest time window, and calculates the variance Var_i of S_i. If at least three sequences' variances are less than the threshold, the current location $L_t(x_t, y_t)$ will be measured by the algorithm of SpotFi. Otherwise, $L_t(x_t, y_t)$ will be measured by the algorithm of Bifrost (refer to Eq. 2).

Algorithm 1: Error reduction using Kalman filter.

Initialize state vector A_0 with the first few points;
for $t = 1, 2, 3, \ldots$ **do**
  Predict the next state $\hat{A}_t^-$;
  Obtain the AoA estimation sequence $S_i = [AoA_1^i\ AoA_2^i\ \ldots\ AoA_n^i]$ from each WiFi AP;
  Calculate the variance Var_i of each sequence S_i;
  Count the number Num of the Var_i higher than $Threshold$;
  if $Num < 3$ **then**
    Determine current obtained frequencies f_r and f_l;
    Calculate the current location $L_t(x_t, y_t)$ by employing the basic localization model of Bifrost;
  end
  else if $Num \geq 3$ **then**
    Calculate the current location $L_t(x_t, y_t)$ by employing the localization algorithm of SpotFi;
  end
  Fuse new estimated location in L_t with predicted results in $\hat{A}_t^-$;
  Output the optimal state $\hat{A}_t$;
end

Finally, the measured current location L_t will be fused with $\hat{A}_t^-$ to output the optimal estimate $\hat{A}_t$, (*i.e.,* the a posteriori state estimate) based on the following formula

$$\hat{A}_t = \hat{A}_t^- + K \cdot (L_t - H \cdot \hat{A}_t^-) \tag{9}$$

where K is the Kalman gain and H is the observation matrix defined by the user.

5 Practical Issues

We complete the design of Bifrost by articulating some practical issues of its applicability.

Selecting the Best WiFi Link. Generally, there will be multiple WiFi APs in many indoor scenarios, no matter LoS or NLoS. In other words, there are many different WiFi links. If the device is able to access multiple WiFi links, we should determine that choosing which one to connect for localization can result in the most accurate results.

In this case, the device can first choose WiFi links that provide higher RSSI, which means that the energy of the corresponding FSDM signals will also be strong. After that, the device can connect to the selected links and run Bifrost algorithm in turn. The link leads to the smallest size of weight matrix G will be chosen for localization because the smaller the size of G, the narrower the range of LoS signals' frequency. Thus, the estimation of LoS signals' frequency and further the localization results are likely to be more accurate.

Reciprocity of LWAs. Recall that we use the WiFi antenna (*e.g.,* dipole antenna) to feed WiFi signals into the LWA to generate FSDM signals. The reverse propagation also exists, which is called the reciprocity of antennas.

However, the energy of these re-radiated signals is very low, because only the FSDM signal with a specific frequency and AoA can be absorbed by LWAs. Thus, the interference they bring is negligible. Besides, we employ an amplifier to only boost signals in the desired propagation path (*i.e.,* from LP antenna to the LWA), while isolating signals in the reverse path.

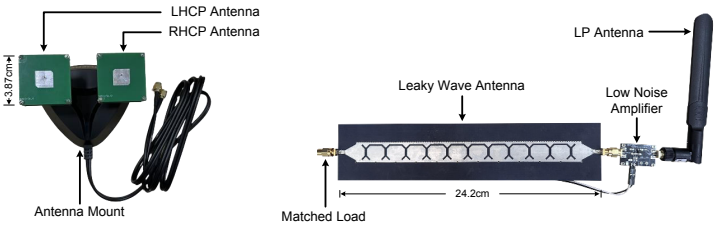

(a) Target. (b) LWA.

Fig. 11. Hardware Settings.

(a) Hall. (b) Corridor. (c) Meeting room. (d) Classroom.

Fig. 12. Experimental scenarios.

Polarization Alteration. If the CP signal reflects off the indoor blockage, its horizontal and vertical components may be introduced a phase shift of π, respectively. This phenomenon is called Half-Wave loss, which will lead to the polarization alteration, *e.g.*, from LHCP to RHCP.

Note that we can deal with this phenomenon via our algorithm shown in Fig. 9. Because the root cause of polarization alteration is the signal reflection, its impact is the same as the multipath effect. Specifically, when the polarization of the signal alters, it indicates that the signal has been reflected on an obstacle and its energy attenuates after reflection. Thus, we can still regard it as the multipath signal and filter it out by analyzing the CSI. Thus, polarization alteration doesn't affect the function and reliability of the localization algorithm.

Interference between LWAs. In the setting of Bifrost, each room is equipped with only one RHCP LWA and one LHCP LWA, respectively. Thus, LWAs sharing the same polarization are inherently separated by walls. Thus, different pairs of LWAs don't interfere with each other.

However, there is a potential concern regarding through-the-wall interference. Note that the strength of these interference signals is significantly weakened after they propagate through walls [16, 18]. As a result, they can hardly be identified as the LoS signals according to our algorithm (Sec. 3.4), and only be filtered out as the multipath signals. Therefore, different pairs of LWAs in different rooms hardly interfere with each other and don't affect the function of the localization.

6 Evaluation

6.1 Implementation and Experimental Methodology

Hardware and software. Our proposed LWA is shown in Fig. 11(b), which is designed to work at 5.17GHz-5.33GHz. The main body of our LWA is 24.2cm × 5.2cm, containing 11 single units designed to ensure most input signals' energy can be leaked out. By switching the feed port, the polarization of the FSDM signal can be altered between LHCP and RHCP. Besides, a low-noise amplifier powered by a small rechargeable battery is utilized to boost the input signal with a 20% duty cycle. To receive the CP FSDM signal, we equip the target with two

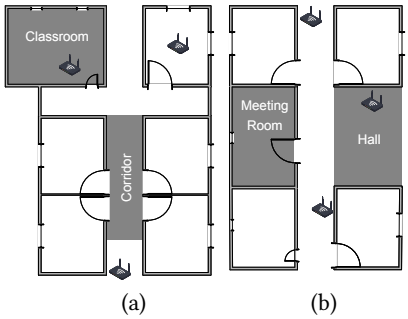

Fig. 13. The realistic indoor AP setting (a) in the corridor and the classroom, and (b) in the hall and the meeting room.

3.87cm × 3.87cm patch antennas, as Fig. 11(a) depicts. One antenna is LHCP, while the other is RHCP, and both are connected to COMFAST AX210 WiFi card [10] on the computer.

We use PicoScenes [20], a WiFi sensing platform, to send WiFi packets at AP with 20dBm, and extract CSI at the target. We run PicoScenes on Ubuntu 20.04, then analyze CSI data and execute the our algorithm on MATLAB 2022b.

Baseline. We compare Bifrost with SpotFi [22], the state-of-the-art indoor WiFi localization technique, under various settings. To ensure the validity of our results, we make our best effort to re-implement SpotFi and ensure fairness through comparison. We evaluate the performance of SpotFi by deploying multiple WiFi APs *strictly based on the real-world settings of WiFi APs*, as Fig. 12 and Fig. 13 shows. We use a laser rangefinder to obtain the ground-truth, including coordinates of the target and LWAs.

Scenarios and deployment. We select four typical indoor scenarios for evaluation (some are shown in Fig. 12), across different sizes and different levels of multipath effect: 1) A small-size hall (6.2m × 4.5m) with few multipath; 2) A long and narrow corridor (7.5m × 2.1m) with few multipath; 3) A small-size meeting room (5.7m × 4.9m) with rich multipath; 4) A large-size classroom (10.6m × 7.1m) with rich multipath. In each scenario, two LWAs are attached to two orthogonal walls. The target device is mounted onto tripods, keeping the height constant across all experiments.

6.2 Overall Performance

In this section, we first evaluate the localization accuracy of Bifrost and SpotFi in real-world settings, where WiFi APs in experiments are deployed at the same positions as those in practice. Then we deploy Bifrost in the meeting room and classroom, where SpotFi doesn't work well, to enhance the performance of SpotFi, so as to see the accuracy improvement brought by Bifrost.

Performance comparison in realistic settings. In reality, most indoor WiFi APs are dispersively deployed at different locations and very likely separated from each other by walls so that LoS paths are usually obstructed. Thus, the target device is hard to establish more than one LoS connection with APs, according to our real-world investigation (*i.e.,* Fig. 2). We evaluate the performance of SpotFi in these practical indoor settings, and also the localization error of Bifrost when deployed in the above-mentioned four scenarios. 50 locations are chosen in each scenario for location estimation. The evaluation results are reported in Fig. 14.

In the hall, both Bifrost and SpotFi are supposed to exhibit the best performance due to the low-level multipath effect, but the median error of SpotFi is 1.23m, which is more than 2× of Bifrost's 0.61m. This is because only one decent LoS signal can be obtained at most locations due to the blockage of walls even though three APs are deployed around. As the pie chart illustrates, SpotFi outperforms Bifrost at only 9 locations. When it comes to

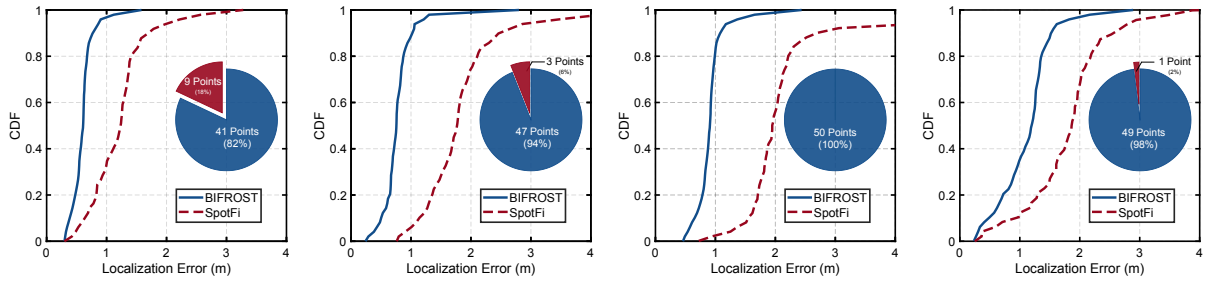

(a) Hall (b) Corridor (c) Meeting room (d) Classroom

Fig. 14. Overall performance of Bifrost and SpotFi across different scenarios (The pie charts represent how many locations where each method shows a lower error).

the corridor scenario, the median error of SpotFi increases to 1.77m because two of the three APs are situated inside rooms so the AoAs obtained by the target are heavily distorted.

Next, we switch to the meeting room where more pronounced multipaths exist. What's worse, there is no AP in the meeting room, more challenging for both two approaches to function. The accuracy of the two approaches is unsurprisingly degraded, where the median error is 1.95m in SpotFi and 0.91m in Bifrost. Similarly, the performance of SpotFi is restrained due to the lack of the LoS signal. Bifrost exhibits acceptable performance in this tough environment and avoids escalation of errors. This can be attributed to two aspects. On one hand, Bifrost can function once the input signal has enough energy, without the need for LoS AP. On the other hand, Bifrost exploits a delicate algorithm to tame the multipath effect. In this scenario, SpotFi doesn't outperform Bifrost on any point.

Finally, we set SpotFi and Bifrost in the large-size classroom with rich multipath. With a LoS AP, the median error of SpotFi is reduced to 1.87m, which is better than that in the meeting room with no LoS AP. By contrast, the median error of Bifrost increases to 1.20m, mainly due to a longer distance between LWAs and WiFi APs and multipath.

Through all experiments in four scenarios, the median error of Bifrost is 0.81m, which is 52.35% less than that of SpotFi (*i.e.,* 1.70m). Bifrost outperforms SpotFi at most locations, except at which the target can obtain 3 LoS signals from 3 APs. However, as shown in Fig. 14, the chance for SpotFi to achieve better performance is less than 7%.

Performance comparison in NLoS scenarios. Then we conduct experiments to demonstrate Bifrost's ability of localization in NLoS scenarios and compare its performance with that of SpotFi.

We deploy the localized target and the LWAs in a hall. As Bifrost only uses one AP to function, we evaluate the performance of Bifrost when this AP is inside and outside the hall (*i.e.,* LoS and NLoS scenarios). The NLoS setting is shown in Fig. 15.

The results in Fig. 16 show that the median errors of Bifrost are 0.61m in LoS and 0.73m in NLoS, respectively. Meanwhile, in the same hall, we also evaluate the performance of SpotFi in LoS and NLoS scenarios, respectively. In the LoS scenario, 3 APs are deployed in the hall and can establish LoS connections with the target. In the NLoS scenario, one of the APs (*i.e.,* AP1) is outside the room, while the other 2 APs (*i.e.,* AP2 and AP3) can connect with the target along the LoS paths. We find that the median error of SpotFi increases from 0.45m in LoS to 1.15m in NLoS. The error may further go beyond 1.6m if only one AP is left in LoS, as reported in [22]. This demonstrates that Bifrost provides relatively stable performance when the WiFi AP is the NLoS scenario. Besides, in NLoS scenarios, Bifrost can achieve more accurate results than SpotFi.

Performance enhancement when Bifrost aids SpotFi. Next, we deploy Bifrost where SpotFi shows poor accuracy to see if Bifrost can aid SpotFi to improve localization accuracy. Actually, it is impossible to

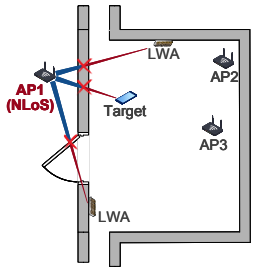

Fig. 15. Deployment of devices in the NLoS settings.

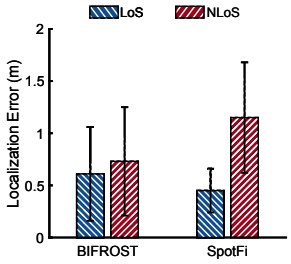

Fig. 16. Performance of Bifrost and SpotFi in the NLoS scenario.

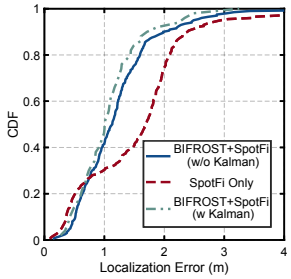

Fig. 17. Performance enhancement brought by Bifrost.

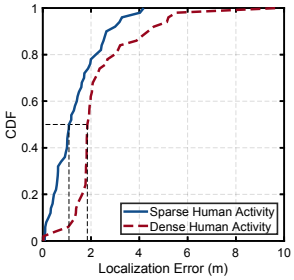

Fig. 18. Impact of the density of daily human activity.

deploy Bifrost everywhere, so we choose the meeting room and classroom where localization accuracy is heavily affected by constrained APs and reports the worst results. Specifically, when the target gets into these two scenarios, its location will be reported by Bifrost. Otherwise, the target keeps using SpotFi for indoor localization.

As shown in Fig. 17, the median localization error is 1.13m when Bifrost aids SpotFi (blue solid line), achieving 33.54% error reduction compared with SpotFi operating independently in all scenarios, which is 1.70m as reported above (red dashed line). Further, we employ our dedicated Kalman filter to reduce the error when Bifrost cooperates with SpotFi. Results show that the median error is reduced to 1.02m (greed dashed line). This indicates that Bifrost can not only work independently, but also enhance localization accuracy and availability of existing WiFi-based indoor localization techniques.

6.3 Impacting Factors

Next, we analyze the impact of three different factors on the performance of Bifrost.

Human activity. The indoor environments exhibit complex dynamics, with the presence of human activity and other mobile objects, which will change the reflection of multipath signals. Such changes can cause the out-of-order variation of CSI, or even block the LoS path of FSDM signals, which will severely affect the AoA and location estimation. Accordingly, we investigate how these activities influence the performance of Bifrost. We deploy LWAs and the target along a pathway between two laboratories and evaluate the localization results during two distinct periods, *5:00 - 7:00 p.m.*, dinner time with dense human activities (approximately 40 people move successively during this period), and *9:30 - 11:30 p.m.*, nightfall with sparse human activities (approximately 15 people move successively during this period). Fig. 18 shows that the median error increases from 1.12m to 1.86m as human activities become denser, indicating that more severe interference is produced in signal propagation.

Transmission power. The default transmission power of AP is 20dBm in our above-mentioned evaluations, and we now vary this value to investigate its impact on localization performance. Moreover, as mentioned before, we can't always guarantee that the WiFi AP establishes LoS path with LWAs, so we also compare the situation of the AP at LoS and NLoS scenarios in each setting of transmission power. We place AP at 2m distance outside the door and the target 2m inside the door, switching between the LoS and NLoS scenarios by opening and closing the door. The transmission power is set to 10dBm, 15dBm and 20dBm, respectively. Results in Fig. 19 show that decreasing the transmission power leads to an increase in the localization error, regardless of whether the AP is at LoS or NLoS. Besides, the errors in LoS scenario are always lower than that of NLoS for the same transmission power.

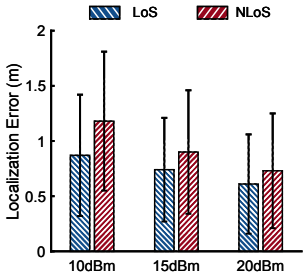

Fig. 19. Impact of the transmission power.

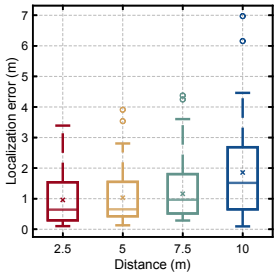

Fig. 20. Impact of distance between AP and LWAs.

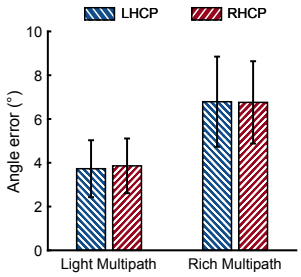

Fig. 21. Impact of the multipath effect.

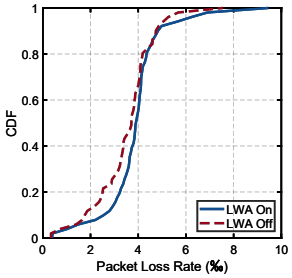

Fig. 22. Impact on the AP and the target of Bifrost.

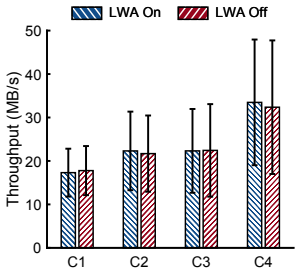

Fig. 23. Impact on other WiFi connections.

However, we also observe that as the transmission power increases, the impact of NLoS on the performance of Bifrost decreases, albeit gradually. Notably, when the transmission power is set at 20dBm, the median errors are 0.61m and 0.73m at LoS and NLoS scenarios, respectively.

Distance between AP and LWAs. The performance of Bifrost may be influenced by the energy of the input WiFi signal fed into LWAs, because it determines the SNR (signal-to-noise ratio) of the FSDM signal. The energy of the input WiFi signal is mainly related to two factors, namely the transmission power and the distance between the AP and LWAs. While the former factor is previously discussed, we here probe into the impact of distance. We carry out the experiments along the corridor and remove the reflectors as far as possible, while the distance is set to 2.5m, 5m, 7.5m, and 10m. Results in Fig. 20 demonstrate that the localization error increases with distance and may even result in outliers. The median errors are 0.63m, 0.65m, and 0.93m in the first three groups of experiments, all of which are below 1m, yet spike to 1.49m in the setting of 10m distance. Despite this, the range of 7.5m is sufficient to cover most rooms, ensuring the feasibility of Bifrost.

Multipath. We examine the AoA estimation accuracy of Bifrost in multipath scenarios. We fix the positions of LWAs and the target, then change the number of indoor objects (*i.e.,* chairs and desks) to create different degrees of multipath. Specifically, two desks are first set in the room to emulate a light multipath environment, and then ten chairs are further added to produce richer signal reflections. The results in Fig. 21 indicate that the AoA estimation accuracy degrades as the multipath is intensified, where the median angle error initially sits around 3.8°, and then increases to around 6.7°. We also note that Bifrost maintains relatively stable performance across different polarizations. The difference between median errors of LHCP and RHCP signals is less than 0.3°, which underscores the robustness of our proposed LWA and localization algorithm.

6.4 Impact on Communication

In this section, we evaluate the impact of deploying Bifrost on the WiFi connections. Firstly, we control the AP to transmit 1000 packets at a 50*ms* interval, and the packet loss rate is recorded in each group of experiments. The results in Fig. 22 show that the median packet loss rates are 3.92‰ and 3.71‰ when the LWA is on and off, respectively. This 0.2‰ difference implies that the function of Bifrost has a negligible influence on the AP-target communication.

Secondly, we place Bifrost's transceiver at an intersection region covered by two commercial APs (AP1 in a classroom and AP2 in a laboratory) with good signal quality. We then use different off-the-shelf smartphones to establish WiFi connections with these APs and record the variation in throughput over 2 hours for each connection (C1: OnePlus 9-AP1, C2: iPhone 13-AP2, C3: OnePlus 9-AP1, and C4: iPhone-13-AP2). The results are shown in Fig. 23. We find that the median throughput degrades 2.7% and 0.4% in C1 and C3, which have nearly no impact on the network quality or user experience. Interestingly, the throughput increases when the LWAs are turned on for C2 and C4. This increase is mainly caused by the changes in wireless channels.

7 Discussion

In this section, we discuss practical issues concerning the applicability and efficacy of Bifrost.

Applicability of Bifrost. Considering that most of the current commercial WiFi devices are equipped with LP antennas, they may be not compatible with Bifrost yet. There are two potential solutions to enhance the applicability of Bifrost. On one hand, some commercial off-the-shelf CP antennas (*e.g.,* CP flat patch antennas [24] of L-com, Inc) are developed to be integrated with existing WiFi APs. Bifrost can be deployed on such devices. On the other hand, in our future work, we will study how to utilize LP rather than CP signals to improve the applicability of Bifrost. To distinguish LWAs using the LP signals, different phase shifts or OOK patterns may be exploited.

Integrating Bifrost with other localization methods. Bifrost is an AoA-based localization approach that can be combined with any other WiFi localization method to improve their accuracy. Specifically, Bifrost can be deployed in areas where the original method shows poor accuracy (*e.g.,* the median error in the areas is higher than that of Bifrost), allowing the device to switch to Bifrost when entering these areas, while continuing to use the original method elsewhere. We demonstrate how to integrate Bifrost with SpotFi, while this methodology can also be applied to other localization methods, such as those based on AoA, ToF, and fingerprint. Note that the current version of Bifrost mainly focuses on localizing static WiFi devices, which has significant applicable value in many applications, *e.g.,* asset management, device finding and location-aware sensing. Users can also combine Bifrost with existing tracking algorithm [26, 38] to enable more applications, such as tracking a device carried by a moving user.

Strategies for LWA deployment. To maintain consistent coverage and ensure accuracy, users should strategically deploy the LWAs in locations that can establish the LoS paths to most of the sensing area. Additionally, if the sensing area changes frequently, placing the LWAs higher up or on the ceiling can help keep a stable localization performance.

Maintenance requirements of LWAs. The rated current of LWAs is 0.86mA. A LWA is powered with a 1600mAh battery and works at 20% duty cycle. So the estimated lifetime of a LWA is over 9302 hours ($\approx$ 387 days) and the maintenance cost is recharging the battery once every 387 days.

Besides, one may be concerned that if multiple LWAs are deployed closely, LWAs with the same polarization will interfere with each other. However, each room only has one RHCP LWA and one LHCP LWA in the setting of Bifrost, so LWAs with the same polarization are separated by walls. Interference signals must propagate through the wall, after which they only have low strength. Therefore, different pairs of LWAs hardly interfere with each other.

Operating in edge cases. The operation of Bifrost relies on the ambient WiFi signals and the identification of LoS FSDM signals. Consequently, areas with sparse WiFi AP coverage or with significant multipath may degrade the performance of Bifrost. The solutions are two-fold. In scenarios with few WiFi APs, users can integrate LWAs with a high-gain amplifier to boost the FSDM signal for stable localization performance. In scenarios with significant multipath, users can carefully choose the location to deploy LWAs to maximize LoS coverage of the sensing area.

8 Related Work

Application of LWA. The work closest to ours is 123-LOC [21], which presents a THz LWA with two perpendicular slots to radiate horizontal and vertical polarized FSDM signals. Range and angle estimation is then performed by the receiver based on the bandwidth and frequencies of received signals. In comparison, Bifrost reduces the impact of multipath and achieves room-scale localization, which is a challenging task for THz signals.

LeakyTrack [12] tracks the object between two LWAs based on the observation that nodal and environmental motion changes the received spectral profile of FSDM signals. [43] investigates the security of THz networks with LWAs and shows that FSDM signals of the LWA can hinder eavesdroppers, *e.g.,* by using a wide-band transmission. [13] studies single-shot link discovery with the help of FSDM signals from the LWA. A receiver can discover the direction of the path from the transmitter in one shot. In contrast to those works that require a specific feeding device for THz LWA, Bifrost operates in the WiFi band and works in a plug-and-play manner.

WiFi-based Indoor Localization. There have been numerous efforts on indoor localization with WiFi [35, 39, 40]. Traditional fingerprint-based techniques have been widely used by mapping the RSS readings from multiple APs with locations [25, 37]. Techniques based on AoA and ToF have become more prevalent recently. For example, ArrayTrack [39] proposes an AoA-based WiFi localization system that incorporates multiple APs and the Multiple Signal Classification (MUSIC) algorithm. SpotFi [22] proposes a MUSIC algorithm to obtain AoA and ToF simultaneously.

Despite such advances, existing methods may chop up the communication link between the target and the AP when the target hops between different APs or channels. In contrast, Bifrost does not interfere with communication links, but only supplements the APs' ability.

9 Conclusion

This paper introduces Bifrost, a low-cost and plug-and-play technique to enhance the availability and accuracy of WiFi localization. It can either aid existing techniques to improve their performance, or operate independently to outperform the state of the arts in arguably realistic indoor settings, without affecting ongoing data communication of WiFi networks. What sets Bifrost apart from other solutions is the exploration in the polarization of wireless signals and the dispersion property of LWAs, which embodies the concept of RF computing [7, 34, 46]. We plan to explore the research space further in this direction.

Acknowledgments

This work is supported by the National Natural Science Foundation of China under grant No. 62425207, No. U21B2007 and No. 62472379

References

[1] Amazon. 2023. Amazon TP-Link AC1200 WiFi Router. https://www.amazon.com/TP-Link-AC1200-Router-Archer-A54/dp/B09G5Y1HWZ/ref=sr_1_1?keywords=wifi+router&qid=1687784198&sr=8-1. Accessed: 2023-06-26.

[2] Amazon. 2023. Amazon TP-Link Smart WiFi 6 Router. https://www.amazon.com/TP-Link-Wireless-AX1500-Wifi-Router/dp/B07ZSDR49S/ref=sr_1_3?keywords=wifi+router&qid=1687784198&sr=8-3. Accessed: 2023-06-26.

[3] Yuanxi Cao and Sen Yan. 2021. A Low-profile High-gain Multi-beam Antenna based on 3D-printed Cylindrical Luneburg Lens. *Microwave and Optical Technology Letters* 63, 7 (2021).
[4] Yuanxi Cao, Sen Yan, and Juan Chen. 2023. An SIW Pillbox-based Compact Dual-polarized Multibeam Antenna with Passive 2-D Beam Scanning Capability. *IEEE Transactions on Circuits and Systems II: Express Briefs* 70, 1 (2023).
[5] Yuanxi Cao, Sen Yan, Wendong Liu, and Jianxing Li. 2023. A Wideband Multibeam Pillbox Antenna Based on Differentially Fed Leaky-wave Array. *IEEE Antennas and Wireless Propagation Letters* 22, 3 (2023).
[6] Roberto Carvalho, Shan-Ho Yang, Yao-Hua Ho, and Ling-Jyh Chen. 2016. Indoor Localization Using FM and DVB-T Signals. In *Proceedings of IEEE CCNC*.
[7] Lili Chen, Wenjun Hu, Kyle Jamieson, Xiaojiang Chen, Dingyi Fang, and Jeremy Gummeson. 2021. Pushing the Physical Limits of IoT Devices with Programmable Metasurfaces. In *Proceedings USENIX NSDI*.
[8] Yulong Chen, Junchen Guo, Yimiao Sun, Haipeng Yao, Yunhao Liu, and Yuan He. 2024. ELASE: Enabling Real-time Elastic Sensing Resource Scheduling in 5G vRAN. In *Proceedings of IEEE/ACM IWQoS*.
[9] Zhe Chen, Guorong Zhu, Sulei Wang, Yuedong Xu, Jie Xiong, Jin Zhao, Jun Luo, and Xin Wang. 2019. M^3: Multipath Assisted Wi-Fi Localization with a Single Access Point. *IEEE Transactions on Mobile Computing* 20, 2 (2019).
[10] COMFAST. 2023. CF-AX210 PRO. http://www.comfast.com.cn/index.php?m=content&c=index&a=show&catid=13&id=123. Accessed: 2023-03-17.
[11] Pei Du and Nirupama Bulusu. 2021. An Automated AR-based Annotation Tool for Indoor Navigation for Visually Impaired People. In *Proceedings of ACM ASSETS*.
[12] Yasaman Ghasempour, Chia-Yi Yeh, Rabi Shrestha, Yasith Amarasinghe, Daniel Mittleman, and Edward W. Knightly. 2020. LeakyTrack: Non-coherent Single-antenna Nodal and Environmental Mobility Tracking with a Leaky-wave Antenna. In *Proceedings of ACM SenSys*.
[13] Yasaman Ghasempour, Chia-Yi Yeh, Rabi Shrestha, Daniel Mittleman, and Edward Knightly. 2020. Single Shot Single Antenna Path Discovery in THz Networks. In *Proceedings of ACM MobiCom*.
[14] Jon Gjengset, Jie Xiong, Graeme McPhillips, and Kyle Jamieson. 2014. Phaser: Enabling Phased Array Signal Processing on Commodity WiFi Access Points. In *Proceedings of ACM MobiCom*.
[15] Baoshen Guo, Weijian Zuo, Shuai Wang, Wenjun Lyu, Zhiqing Hong, Yi Ding, Tian He, and Desheng Zhang. 2022. Wepos: Weak-supervised Indoor Positioning with Unlabeled WiFi for On-demand Delivery. *Proceedings of ACM IMWUT* 6, 2 (2022), 1–25.
[16] Xiuzhen Guo, Yuan He, Jing Nan, Jiacheng Zhang, Yunhao Liu, and Longfei Shangguan. 2024. A low-power demodulator for LoRa backscatter systems with frequency-amplitude transformation. *IEEE/ACM Transactions on Networking* (2024).
[17] Xiuzhen Guo, Yuan He, Longfei Shangguan, Yande Chen, Chaojie Gu, Yuanchao Shu, Kyle Jamieson, and Jiming Chen. 2024. Mighty: Towards Long-Range and High-Throughput Backscatter for Drones. *IEEE Transactions on Mobile Computing* (2024).
[18] Xiuzhen Guo, Yuan He, Jiacheng Zhang, Yunhao Liu, and Longfei Shangguan. 2024. Towards Programmable Backscatter Radio Design for Heterogeneous Wireless Networks. *IEEE/ACM Transactions on Networking* (2024).
[19] David R Jackson, Christophe Caloz, and Tatsuo Itoh. 2012. Leaky-wave Antennas. *Proc. IEEE* 100, 7 (2012).
[20] Zhiping Jiang, Tom H. Luan, Xincheng Ren, Dongtao Lv, Han Hao, Jing Wang, Kun Zhao, Wei Xi, Yueshen Xu, and Rui Li. 2022. Eliminating the Barriers: Demystifying Wi-Fi Baseband Design and Introducing the PicoScenes Wi-Fi Sensing Platform. *IEEE Internet of Things Journal* 9, 6 (2022).
[21] Atsutse Kludze, Rabi Shrestha, Chowdhury Miftah, Edward Knightly, Daniel Mittleman, and Yasaman Ghasempour. 2022. Quasi-optical 3D Localization Using Asymmetric Signatures above 100 GHz. In *Proceedings of ACM MobiCom*.
[22] Manikanta Kotaru, Kiran Joshi, Dinesh Bharadia, and Sachin Katti. 2015. SpotFi: Decimeter Level Localization Using WiFi. In *Proceedings of ACM SIGCOMM*.
[23] Vikram Kumar, Reza Arablouei, Raja Jurdak, Branislav Kusy, and Neil W Bergmann. 2017. RSSI-based Self-localization with Perturbed Anchor Positions. In *Proceedings of IEEE PIMRC*.
[24] L-com. 2023. Circular Polarized Patch Antenna. https://www.l-com.com/wireless-antenna-24-ghz-8-dbi-circular-polarized-rh-flat-patch-antennas. Accessed: 2023-10-03.
[25] Danyang Li, Jingao Xu, Zheng Yang, Chenshu Wu, Jianbo Li, and Nicholas D Lane. 2021. Wireless Localization with Spatial-temporal Robust Fingerprints. *ACM Transactions on Sensor Networks* 18, 1 (2021), 1–23.
[26] Xiang Li, Daqing Zhang, Qin Lv, Jie Xiong, Shengjie Li, Yue Zhang, and Hong Mei. 2017. IndoTrack: DevicefFree Indoor Human Tracking with Commodity Wi-Fi. *Proceedings of ACM IMWUT* 1, 3 (2017).
[27] Francesco Monticone and Andrea Alu. 2015. Leaky-wave Theory, Techniques, and Applications: From Microwaves to Visible Frequencies. *Proc. IEEE* 103, 5 (2015).
[28] Sujay Narayana, Vijay Rao, R Venkatesha Prasad, Ajay K Kanthila, Kavya Managundi, Luca Mottola, and T Venkata Prabhakar. 2020. LOCI: Privacy-aware, Device-free, Low-power Localization of Multiple Persons Using IR Sensors. In *Proceedings of ACM/IEEE IPSN*.
[29] Dan Simon. 2001. Kalman filtering. *Embedded systems programming* 14, 6 (2001), 72–79.
[30] Elahe Soltanaghaei, Avinash Kalyanaraman, and Kamin Whitehouse. 2018. Multipath Triangulation: Decimeter-level WiFi Localization and Orientation with a Single Unaided Receiver. In *Proceedings of ACM MobiSys*.

[31] Yimiao Sun, Yuan He, Yang Zou, Jiaming Gu, Xiaolei Yang, Jia Zhang, and Ziheng Mao. 2025. A Survey of mmWave Backscatter: Applications, Platforms, and Technologies. *Comput. Surveys* (2025).
[32] Yimiao Sun, Weiguo Wang, Luca Mottola, Zhang Jia, Ruijin Wang, and Yuan He. 2024. Indoor Drone Localization and Tracking Based on Acoustic Inertial Measurement. *IEEE Transactions on Mobile Computing* 23, 6 (2024), 7537–7551.
[33] Yimiao Sun, Weiguo Wang, Luca Mottola, Ruijin Wang, and Yuan He. 2022. AIM: Acoustic Inertial Measurement for Indoor Drone Localization and Tracking. In *Proceedings of ACM SenSys*.
[34] Yimiao Sun, Weiguo Wang, Luca Mottola, Ruijin Wang, and Yuan He. 2023. BIFROST: Reinventing WiFi Signals Based on Dispersion Effect for Accurate Indoor Localization. In *Proceedings of ACM SenSys*.
[35] Ju Wang, Hongbo Jiang, Jie Xiong, Kyle Jamieson, Xiaojiang Chen, Dingyi Fang, and Binbin Xie. 2016. LiFS: Low Human-effort, Device-free Localization with Fine-grained Subcarrier Information. In *Proceedings of ACM MobiCom*.
[36] Weiguo Wang, Yuan He, Meng Jin, Yimiao Sun, and Xiuzhen Guo. 2023. Meta-Speaker: Acoustic Source Projection by Exploiting Air Nonlinearity. In *Proceedings of ACM MobiCom*.
[37] Chenshu Wu, Jingao Xu, Zheng Yang, Nicholas D Lane, and Zuwei Yin. 2017. Gain without Pain: Accurate WiFi-based Localization Using Fingerprint Spatial Gradient. *Proceedings of ACM IMWUT* 1, 2 (2017), 1–19.
[38] Yaxiong Xie, Jie Xiong, Mo Li, and Kyle Jamieson. 2019. md-Track: Leveraging Multi-dimensionality for Passive Indoor Wi-Fi Tracking. In *Proceedings of ACM MobiCom*.
[39] Jie Xiong and Kyle Jamieson. 2013. ArrayTrack: A Fine-grained Indoor Location System. In *Proceedings of USENIX NSDI*.
[40] Jie Xiong, Karthikeyan Sundaresan, and Kyle Jamieson. 2015. ToneTrack: Leveraging Frequency-agile Radios for Time-based Indoor Wireless Localization. In *Proceedings of ACM MobiCom*.
[41] Feng Xu and Ke Wu. 2013. Understanding Leaky-wave Structures: A Special Form of Guided-wave Structure. *IEEE Microwave Magazine* 14, 5 (2013).
[42] Yu Yang, Yi Ding, Dengpan Yuan, Guang Wang, Xiaoyang Xie, Yunhuai Liu, Tian He, and Desheng Zhang. 2020. Transloc: Transparent Indoor Localization with Uncertain Human Participation for Instant Delivery. In *Proceedings of ACM MobiCom*.
[43] Chia-Yi Yeh, Yasaman Ghasempour, Yasith Amarasinghe, Daniel M Mittleman, and Edward W Knightly. 2020. Security in Terahertz WLANs with Leaky Wave Antennas. In *Proceedings of ACM WiSec*.
[44] Xianan Zhang, Wei Wang, Xuedou Xiao, Hang Yang, Xinyu Zhang, and Tao Jiang. 2020. Peer-to-Peer Localization for Single-antenna Devices. *Proceedings of ACM IMWUT* 4, 3 (2020), 1–25.
[45] Zhenyong Zhang, Shibo He, Yuanchao Shu, and Zhiguo Shi. 2019. A Self-evolving WiFi-based Indoor Navigation System Using Smartphones. *IEEE Transactions on Mobile Computing* 19, 8 (2019), 1760–1774.
[46] Yang Zou, Xin Na, Yimiao Sun, and Yuan He. 2024. Trident: Interference Avoidance in Multi-Reader Backscatter Network via Frequency-Space Division. *IEEE/ACM Transactions on Networking* (2024).

Received 4 September 2024; revised 13 January 2025; accepted 16 March 2025